Modelling stenosis development in the carotid artery at the early stages of stenosis development

A.C.Stamou*, J.M.Buick**

*Faculty of Engineering and Computing, Coventry University, Priory Street, Coventry CV1 5FB, UK
**School of Engineering, Anglesea Building, Anglesea Road University of Portsmouth, Portsmouth, PO1 3DJ, UK

Abstract: A numerical model is used to simulate the development of a stenosis in the carotid artery where the stenosis forms in regions of stagnant flow. The blood flow properties are computed here using the Lattice Boltzmann Method. The stenosed geometry is presented and found to be consistent with stenosed artery profiles from the literature. Flow fields are also presented which indicate that the flow in the stenosed artery is also consistent with observations form the literature.

Keywords: Stenosis development; Blood flow modelling; Atheroscerosis; lattice Boltzmann Method; arterial wall movement; stagnation

NOTATION

$\mathbf{e}_i$	Grid link
$f_i(\mathbf{x},t)$	Distribution function
$f_i^{(eq)}(\mathbf{x},t)$	Equilibrium distribution function
h	Stenosis development step
i	Lattice label
N	Number of stagnant sites
SI	Stagnation index
T_s	Number of sites, originally in the blood flow, encroached by the developing stenosis
T	Period
t	Time
$\mathbf{u}$	Velocity
w_i	Weight function
$\mathbf{x}$	Position
ρ	Density
Ω_i	Collision function
ω	Vorticity

INTRODUCTION

Atherosclerosis is one of the major causes of ischemic stroke as it can drive the narrowing of the blood vessels due to a built-up of plaque [1]. There is a mass of evidence suggesting that atherosclerosis develops in regions where the velocity and wall shear stress are low [2-4]. Here we consider how the development of the stenosis affects the haemodynamic characteristics of the carotid artery. The blood flow is simulated using the Lattice Boltzmann Model (LBM). The LBM is relatively novel technique to simulate fluid flow and is based on a mesoscopic kinematic approach. LBM simulations have been considered where the blood flow affects a change in the boundary geometry. It has been applied [5, 6] for blood clotting, either on a backward facing step or a pre-existing idealized stenosis [7]. We simulate the development of the stenosis using a model based on [8], where here the stenosis develops in regions of stagnant flow. The sites of maximum stagnation are assumed as the most susceptible regions to the development of the stenosis

METHOD

The simulations are performed using the LBM to simulate the blood flow and using a stenosis growth model to simulate the development of the stenosis.

LBM

In the LBM [9] the particle distributions, $f_i(\mathbf{x}, t)$ at point $\mathbf{x}$, at time t, are confined to move synchronously on a regular lattice. The distribution functions interact on the lattice in such a way that they conserve mass and momentum, and they preserve isotropy and Galilean invariance. The D2Q9 LBM, used in this study, evolves according to the kinetic equation [9, 10]:

$$f_i(\mathbf{x} + \mathbf{e}_i, t + 1) = f_i(\mathbf{x}, t) + \Omega_i(\mathbf{x}, t) \quad [1]$$

where $i = 0, 1, \ldots, 8$ labels the link directions of the underlying grid, given by:

$$\begin{aligned} \mathbf{e}_0 &= (0,0) \\ \mathbf{e}_i &= \left(\cos\left(\frac{\pi}{2}(i-1)\right) \sin\left(\frac{\pi}{2}(i-1)\right)\right) \text{ for } i = 1,2,3,4 \\ \mathbf{e}_i &= \sqrt{2}\left(\cos\left(\frac{\pi}{2}(i-1) + \frac{\pi}{4}\right) \sin\left(\frac{\pi}{2}(i-1)\right) + \frac{\pi}{4}\right) \text{ for } i = 5,6,7,8, \end{aligned} \quad [2]$$

f_i is the distribution function for each of the discrete link directions and Ω_i is the collision operator. The fluid density, ρ, and velocity, **u,** can be calculated from the distribution functions at each node by:

$$\rho = \sum_i f_i \text{ and } \rho\mathbf{u} = \sum_i f_i \mathbf{e}_i . \quad [3]$$

The collision operator, Ω_i , is given by the Bhatnaghar-Gross-Krook approximation [10], as:

$$\Omega_i = -\frac{1}{\tau}\left[f_i(\mathbf{x}, t) - f_i^{eq}(\mathbf{x}, t)\right] \quad [4]$$

where τ is the relaxation time and $f_i^{eq}(\mathbf{x}, t)$ is the equilibrium value of the distribution function:

$$f_i^{eq}(\mathbf{x}, t) = w_i \rho \left(1 + 3\mathbf{e}_i \cdot \mathbf{u} + \frac{9}{2}(\mathbf{e}_i \cdot \mathbf{u})^2 - \frac{3}{2}\mathbf{u}^2\right), \quad [5]$$

where $w_0 = \frac{4}{9}$, $w_1 = w_2 = w_3 = w_4 = \frac{1}{9}$ and $w_5 = w_6 = w_7 = w_8 = \frac{1}{36}$.

A sub-grid extrapolation boundary scheme [11] is applied at the solid boundaries and the cardiac pulse is introduced at the inflow boundary. The form of the pulse is presented in the results section.

Stenosis Growth Model

The development of the stenosis is modelled following [8], where the artery wall is adjusted by a small step, set here to be 0.5 of a lattice spacing, each period of motion; at a position determined by the local haemodynamic properties. Here the position for the development of the stenosis is selected based on the Stagnation Index:

$$SI = N/T \quad [6]$$

where T is the period of the cardiac pulse and N is the number of time-steps in a period when the near-wall velocity (defined to be the velocity one lattice spacing from the wall) at a given site is less than 1% of the average near-wall velocity, over the whole of the wall, a period earlier. The position selected, after each period, for the stenosis to develop, is the wall point where SI is maximum.

RESULTS

As observed in [8], the stenosis is formed in layers which are built up on the outer walls of the External Carotid Artery (ECA) and the Internal Carotid Artery (ICA). After each layer is completed a new layer starts, either on the same artery wall or on the opposite wall. This is shown in Figure 1 at times when a switch occurs between the ICA, on the right of the image, and the ECA, shown on the left.

The layers are depicted in terms of T_s which represents the number of grid sites, originally in the blood flow region, which have been encroached by the growing stenosis. T_s gives a measure of the level of stenosis development. The development occurs on the ECA below the bifurcation, while in the ICA the stenosis occurs from slightly below the bifurcation and extends significantly in to the ICA. Although the geometry of a stenosis can vary significantly from patient to patient, the profile shown in Figure 1 has geometrical similarities to some imaged stenosed arteries [12, 13].

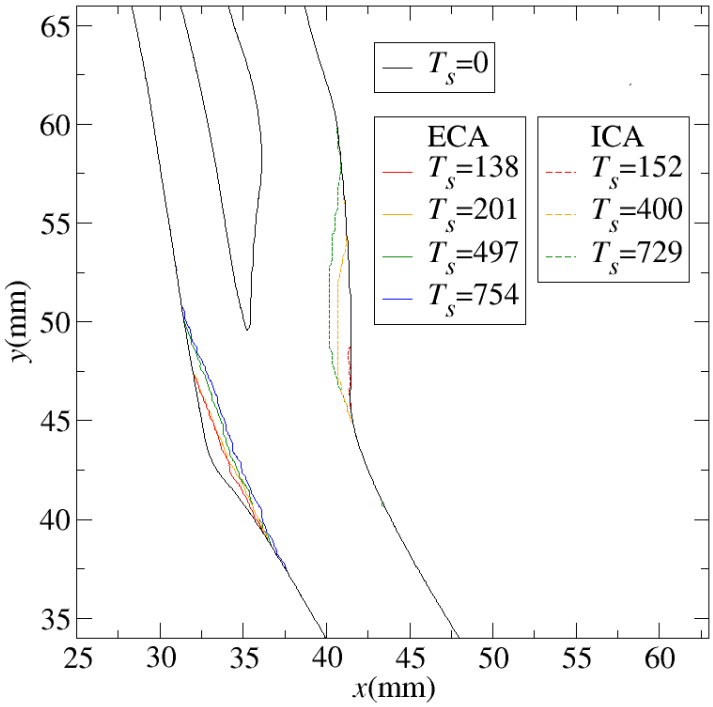

Figure 1. The development of the stenosis in layers

Flow profiles

The effect of the stenosis growth on the blood flow for a stenosed artery (corresponding to T_s = 754 in Figure 1) is shown in Figure 2 for the velocity and Figure 3 for the vorticity, where the stenosed artery is shown on the left and the corresponding healthy artery is shown on the right. The profiles are shown at t = 4T/66 (parts a and b) corresponding to the acceleration phase; t = 7T/66 (parts c and d) corresponding to approximately the peak velocity; and t = 12T/66 (parts e and f) corresponding to the deceleration phase.

In Figures 2 and 3, the driving pulse and healthy geometry are shown as an insert in each figure, while the pulse phase and the stenosed geometry are depicted in the inserts by the red dot and the red geometry respectively.

A higher velocity is observed in both the ICA and the ECA for the stenosed case, relative to the healthy artery. This is in agreement with other studies [14, 15] which predicted a high velocity jet at the base of the ICA and ECA. Significant vorticity develops in the healthy artery towards the bottom of both the ICA and ECA. This can be seen to develop at the peak flow in Figure 3d and fully develop during the deceleration phase, Figure 3f. In contrast, the simulation results for the stenosed artery

(Figure 3 c and e) show that the vortex motion is no longer present in the artery. Figure 1, shows that the region where the vortex motion develops in the healthy artery corresponds to the region where the stenosis forms. The change in the artery geometry in this region explains this change in the blood flow. This is in accordance with earlier observations [15] reported in the literature.

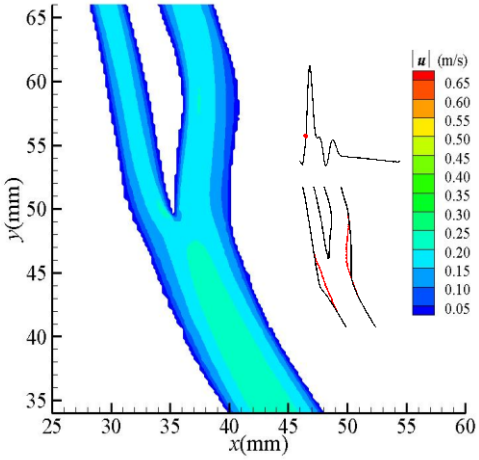

Figure 2a. Stenosed artery velocity field at t=4T/66

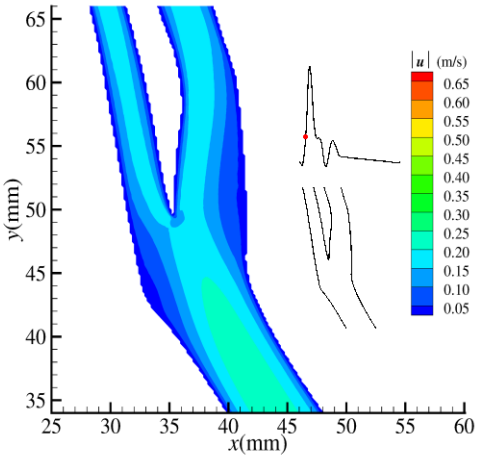

Figure 2b. Healthy artery velocity field at t=4T/66

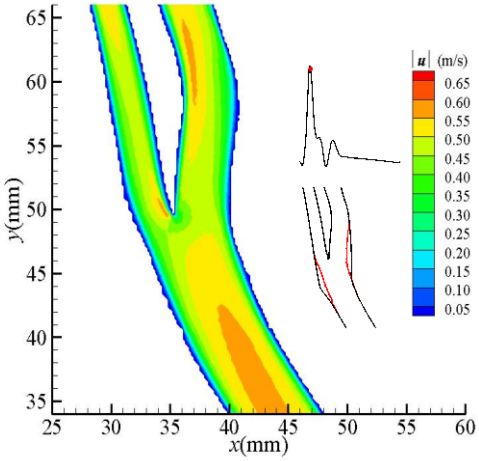

Figure 2c. Stenosed artery velocity field at t=7T/66

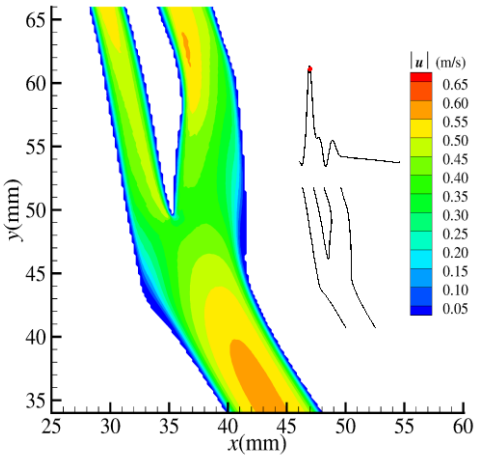

Figure 2d. Healthy artery velocity field at t=7T/66

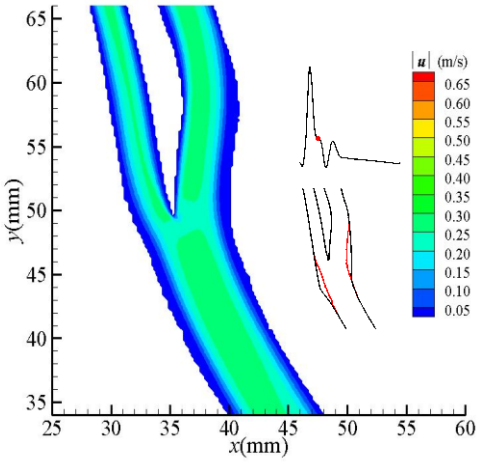

Figure 2e. Stenosed artery velocity field at t=12T/66

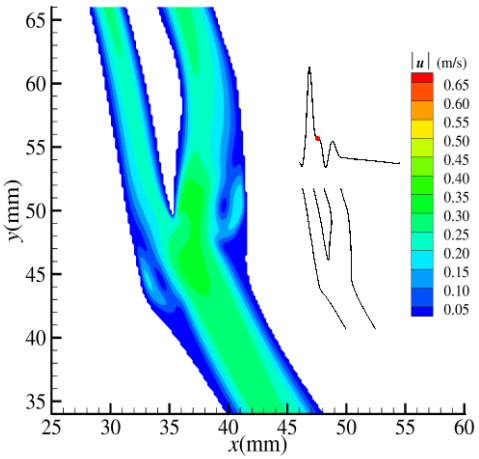

Figure 2f. Healthy artery velocity field at t=12T/66

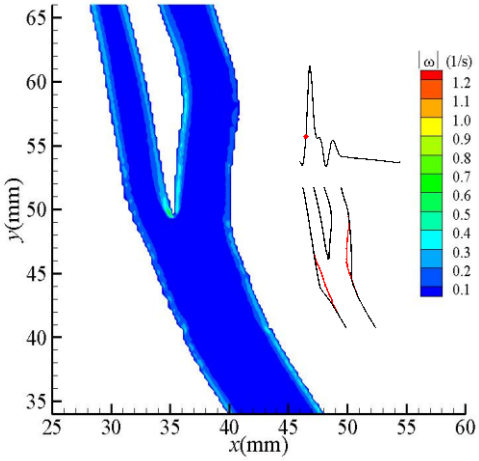

Figure 3a. Stenosed artery vorticity field at t=4T/66

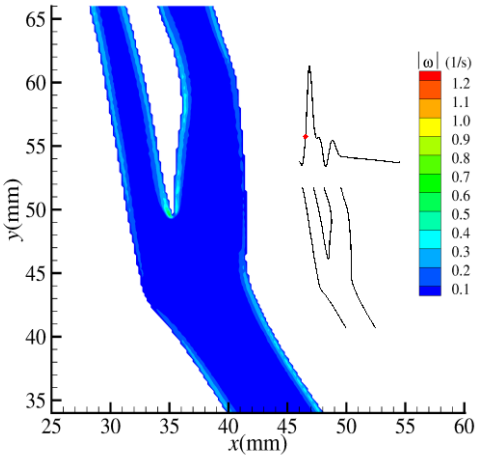

Figure 3b. Healthy artery vorticity field at t=4T/66

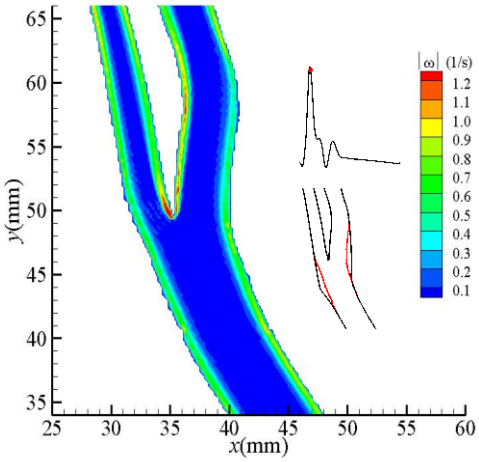

Figure 3c. Stenosed artery vorticity field at t=7T/66

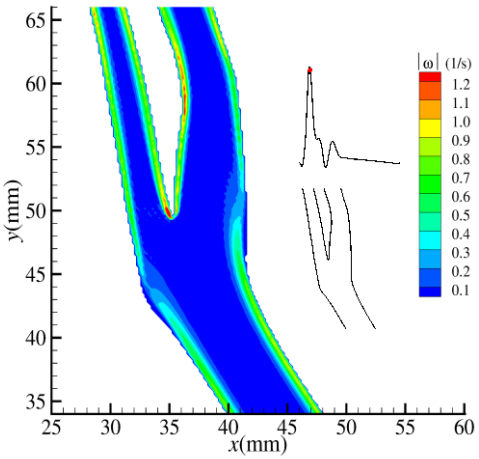

Figure 3d. Healthy artery vorticity field at t=7T/66

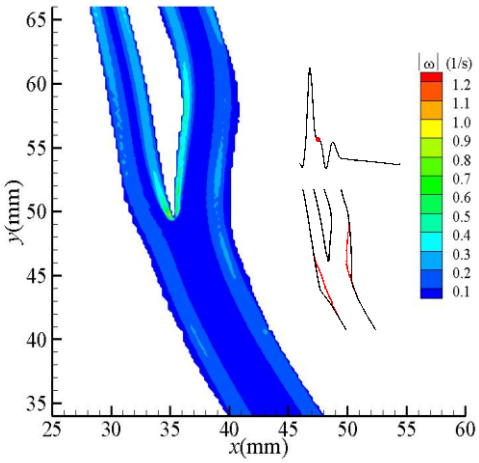

Figure 3e. Stenosis artery vorticity field at t=12T/66

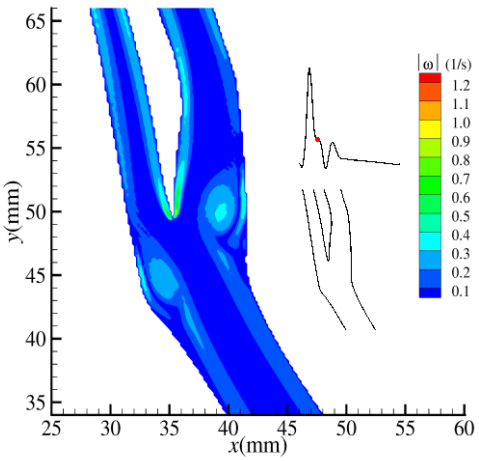

Figure 3f. Healthy artery vorticity field at t=12T/66

CONCLUSION

A numerical model for stenosis growth has been considered. The position of the stenosis has been simulated here based on regions of flow stagnation. This is based on the observation that regions of low velocity have been considered as the prone sites to the atherosclerosis. The stenosis formed on the outer wall of both the ICA and the ECA in the region where vortex motion develops in the healthy artery. This is consistent with regions where stenosis formation has been observed in the literature. The changing flow patterns in the artery with the formed stenosis were shown to be consistent with the literature. In particular an increased velocity was observed in both the ICA and the ECA. Additionally the vortices which were observed in the healthy artery were no longer present once the stenosis had formed. The results suggest that the stagnation model provides a realistic approach to simulating stenosis growth.

REFERENCES

1 A Alwan, 'Global status report on noncommunicable diseases, 2010' World Health Organization, 2010.

2 A Gnasso, C Irace, C Carallo, M S De Franceschi, C Motti, P L Mattioli, and A Pujia, 'In vivo association between low wall shear stress and plaque in subjects with asymmetrical carotid atherosclerosis' Stroke, 1997 28 (5) 993–998.

3 P H Stone, A U Coskun, S Kinlay, M E Clark, M Sonka, A Wahle, O J Ilegbusi, Y Yeghiazarians, J J Popma, J Orav, et al 'Effect of endothelial shear stress on the progression of coronary artery disease, vascular remodeling, and in-stent restenosis in humans in vivo 6-month follow-up study' Circulation, 2003 108 (4) 438–444.

4 Y S. Chatzizisis, A Umit Coskun, M Jonas, E R. Edelman, C L.Feldman, and P H. Stone 'Role of endothelial shear stress in the natural history of coronary atherosclerosis and vascular remodelling molecular, cellular, and vascular behaviour' Journal of the American College of Cardiology, 2007 49 (25) 2379–2393.

5 M Tamagawa, H Kaneda, M Hiramoto, and S Nagahama 'Simulation of thrombus formation in shear flows using Lattice Boltzmann Method' Artificial Organs, 2009 33 (8) 604–610.

6 J Bernsdorf, S E Harrison, S M Smith, P V Lawford, and D R Hose 'Applying the Lattice Boltzmann technique to biofluids: A novel approach to simulate blood coagulation' Computers & Mathematics with Applications, 2008 55 (7) 1408–1414.

7 J Boyd and J M Buick 'Three-dimensional modelling of the human carotid artery using the lattice Boltzmann method: I. Model and velocity analysis' Physics in Medicine and Biology, 2008 53 (20) 5767–5779.

8 A. C. Stamou and J. M. Buick 'An LBM based model for initial stenosis development in the carotid artery' Journal of Physics A, In Press.

9 S. Chen and G.D. Doolen 'Lattice Boltzmann Method for Fluid Flows' Annual Review of Fluid Mechanics, 1998 20 329–364.

10 P L Bhatnagar, E P Gross and M Krook 'A model for collision processes in gases: I. Small amplitude processes in charged and neutral one-component system' Phys Rev, 1954 94 511–525.

11 Z Guo, C Zheng, and B Shi 'An extrapolation method for boundary conditions in lattice Boltzmann method' Physics of Fluids, 2002 14 (6) 2007–2010.

12 W Steinke, C Kloetzsch, and M Hennerici 'Carotid artery disease assessed by color Doppler flow imaging: correlation with standard Doppler sonography and angiography' American Journal of Neuroradiology, 1990 11 (2) :259–266.

13 M Anzidei, A Napoli, B C Marincola, M A Kirchin, C Neira, D Geiger, F Zaccagna, C Catalano, and R Passariello 'High-resolution steady state magnetic resonance angiography of the carotid arteries: are intravascular agents necessary?: feasibility and preliminary experience with gadobenate dimeglumine' Investigative Radiology, 2009 44 (12) 784–792.

14 T L Poepping, N Nikolov, N Rankin, M Lee, and D Holdsworth 'An in vitro system for Doppler ultrasound flow studies in the stenosed carotid artery bifurcation' Ultrasound in Medicine & Biology, 2002 28 (4) 495–506.

15 D A Steinman, T L Poepping, M Tambasco, R N Rankin, and D W Holdsworth 'Flow patterns at the stenosed carotid bifurcation: Effect of concentric versus eccentric stenosis' Annals of Biomedical Engineering, 2000 28 (4) 415–423.